Electronic supporting information for

Characterizing and Understanding the Photovoltage in n-Si/Au Light-Addressable Electrochemical Sensors

Armeen Hussain,[a,c] Kayla M. Mancini,[a,c] Yousef Khatib,[a] and Glen D. O'Neil*[a,b]

[a.] Department of Chemistry and Biochemistry, Montclair State University, Montclair, NJ, United States 07043
[b.] Sokol Institute for Pharmaceutical Life Sciences, Montclair State University, Montclair, NJ, United States 07043
[c.] These authors contributed equally.

Table of contents

Section S1. Experimental section

Materials and solutions. Sodium hexachloroiridate(III)chloride hydrate ($IrCl_6^{3-}$; 98%), tris(2,2′-bipyridyl)dichlororuthenium(II) hexahydrate ($Ru(bpy)_3^{2+}$; 99.95%), and methyl viologen dichloride hydrate (MV^{2+}; 98%) were from Sigma Aldrich; potassium ferricyanide ($K_3Fe(CN)_6$; >99%), sodium hexachloroiridate (IV) ($IrCl_6^{2-}$; 99.9%), ferrocene methanol (FcMeOH; 97%), and hexamine ruthenium(III) chloride ($Ru(NH_3)_6^{3+}$; 97%) were from Acros Organics; NH_4F (40% m/m solution; semiconductor grade) was from Honeywell; potassium nitrate (KNO_3) and potassium ferrocyanide trihydrate were from Fisher Scientific and were ACS Reagent Grade. All solutions were prepared with 18.2 MΩ•cm water purified with a Millipore Simplicity benchtop system.

500 µm thick single-side polished Si (100) wafers were obtained from Pure Wafer (San Jose, CA). Low-doped n-type wafers were doped with phosphorous and had a resistivity of 1-5 Ω•cm; highly doped p+-Si wafers were doped with boron and had a resistivity <0.005 Ω•cm. Indium wire (99.99%) and copper wire (1mm; 99.9%) were from Alfa Aesar. 3M 470 electroplating tape was from Uline.

Fabrication of n-Si/Au and n-Si/Pt LAE sensors. LAE sensors were fabricated according to our previous reports,[1–3] based on a protocol from Allongue et al.[4] 100 mm n- and p+-Si wafers were broken down into 1 cm by 1 cm pieces by scoring the backside of the wafer and breaking along a straight edge. Si dust was removed from the samples using compressed air. The Si samples were cleaned in 105ºC Piranha solution (3 to 1 v/v mixture of concentrated H_2SO_4 to 30% (m/m) H_2O_2) for 30 minutes. The samples were rinsed thoroughly using 18.2 MΩ•cm water. *Caution: Piranha solution is extremely reactive towards organic compounds. Extreme care should be taken when handling and disposing of Piranha solution.* Back contacts were applied by soldering a copper wire to the unpolished side using indium solder after removing the oxide by scratching with a diamond-tipped pen or etching with 40% NH_4F for 10 minutes. Each sensor was sealed in 3M electroplating tape with a 3 mm opening on the polished front side cut using a GlowForge CO_2 laser cutter. Burn marks from the lasering were removed by washing the surface of the plating tape with isopropanol or acetone and wiping dry with a Kimwipe.

Before electrodeposition, each LAE sensor was etched in 40% NH_4F (previously de-oxygenated for 30 minutes with bubbling Ar), rinsed thoroughly with 18.2 MΩ•cm water, and immersed in the electrodeposition solution as quickly as possible. The electrodeposition solution contained 0.5 mM $HAuCl_4$ or 0.5 mM H_2PtCl_6, 0.1 M K_2SO_4, 1 mM KCl, and 1 mM H_2SO_4. The Si electrodes were biased before immersion into the electrodeposition solution to limit the growth of SiOx and prevent the electroless deposition of the metal. Unless otherwise stated electrodeposition was carried out with a constant electrodeposition potential, E_{dep}, of –1.945 V vs. SCE for 300 s.

Figure S1. Schematic showing the fabrication of n-Si/metal LAE sensors prepared using electrodeposition.

Photoelectrochemical measurements. Photoelectrochemical experiments were performed using a CH Instruments 660C or 760E in a 30 mL electrochemical cell with a borosilicate glass window in a three-electrode configuration. A saturated calomel electrode (SCE) or Ag/AgCl (saturated KCl) was used as the reference and a Pt wire or glassy carbon rod was used counter electrode. Illumination was provided using a white light LED from AM Scope with a calibrated intensity of 85 mW cm^{-2}. During these measurements, care was taken to ensure that the position of the electrode relative to the light source was constant. The white light was calibrated using a USB power meter from Thorlabs (PM16-122). All optical components were purchased from Thorlabs and were housed inside a custom-built dark box to

eliminate ambient light. All voltammetric data is presented in the IUPAC convention, with anodic currents positive and cathodic currents are negative.

X-ray photoelectron spectroscopy (XPS). XPS was performed on a Thermo Scientific K-Alpha XPS at the Surface Analysis Facility at the University of Delaware. Survey scans were conducted over the range 0 to 1360 eV. Single-element scans for Au, Si, and C were also performed.

Atomic force microscopy (AFM). AFM images were collected on a Dimension Icon microscope (Bruker, USA) with a NanoScope6 controller operated in ScanAsyst mode. All images were acquired using silicon nitride SCANASYST-AIR-HPI probes ($k = 0.25$ N/m; $f = 55$ kHz; radius ~ 7 nm). Images were collected with an imaging rate of 0.5 Hz and 512 samples per line. Samples were mounted on a stainless steel disk using double-sided tape and attached to the stage with a magnetic sample holder. The entire scanning assembly was placed on an active vibration isolation table pressured at 80 psi and housed inside an insulated Faraday cage with thermal and acoustic noise insulation.
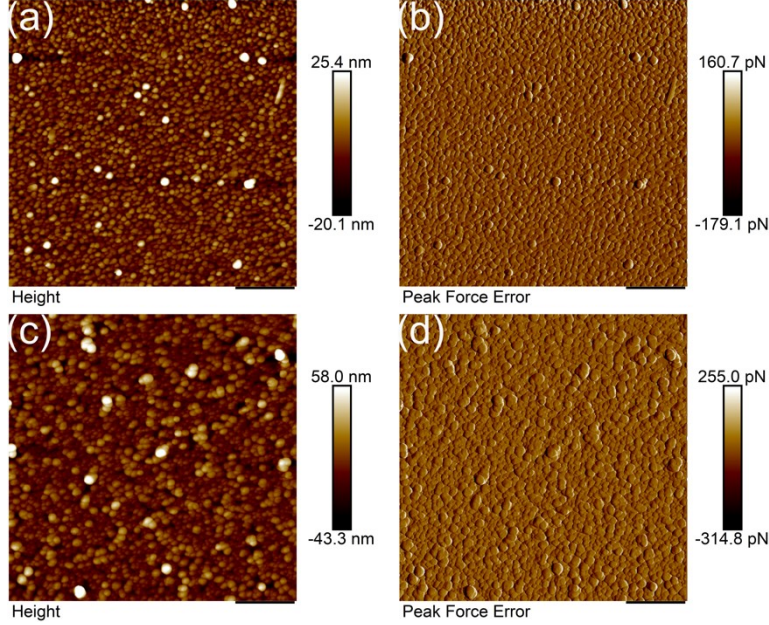
Section S2. Physical and electrochemical characterization of n-Si/Au LAE sensors

Physical characterization of n-Si/Au LAE sensors. Figure S2a shows the XPS survey spectra of an n-Si/Au LAE sensor. We identified elemental peaks for carbon, gold, oxygen, and silicon in the spectra, as displayed in Figure S2a. We performed single-element scans of the Si 2p and Au 4f regions. Figure S2b shows the Si 2p peaks with two clear peaks at 99.2 and 103.1 eV corresponding to elemental Si and SiOx species, respectively. The presence of the oxide does not seem to impact the electrochemistry (see, for instance, Figure S5 below). Figure S2c shows the Au $4f_{5/2}$ and $4f_{7/2}$ spectra at 87.7 and 84.0 eV, respectively. These data are consistent with the formation of gold nanoparticle films.
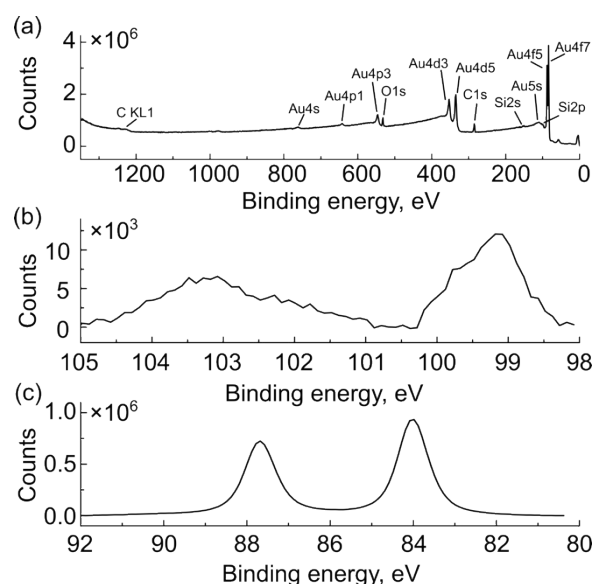
Figure S2. Elemental characterization of n-Si/Au LAE sensor using XPS. (a) Survey scan; (b) Si 2p region; (c) Au 4f region.

We characterized the surface morphology of the sensors using AFM. Figures S3a and S3c show AFM height images (3 μm × 3 μm) of n-Si/Au and p$^+$Si/Au electrodes, respectively, prepared from an electrolyte containing 0.5 mM HAuCl$_4$, 0.1 M K$_2$SO$_4$, 1 mM KCl, and 1 mM H$_2$SO$_4$. Both sets of electrodes show high-density films of nanoparticles that are tens of nm in size. For comparison, Figures S3b and S3d show AFM peak force error images of n-Si/Au and p$^+$Si/Au electrodes, respectively. These images are similar to Figures S3a and S3b, but show more contrast.

Figure S3. Atomic force microscopy characterization of Si/Au LAE sensors acquired in ScanAsyst mode. (a) Height and (b) peak force error images of n-Si/Au LAE sensors. (c) Height and (d) peak force error images of p⁺-Si/Au control sensors. All images are 3 μm × 3 μm.

Electrochemical characterization of n-Si/Au LAE sensors. EIS was used to estimate the band energetics of the n-Si/Au LAE sensors. The electrochemical cell was housed inside a lab-built dark box. These measurements are important for semiconductor/metal LAE sensors because they elucidate the potential window over which the sensors will be "light addressable".[5] Figure S4 shows plots of the reciprocal square space charge capacitance versus applied potential (i.e., Mott-Schottky plots) for n-Si/Au LAE sensors in contact with three different redox species: (a) $IrCl_6^{4-}$, (b) FcMeOH, (c) $Ru(NH_3)_6^{3+}$. All solutions also contained 0.1 M KNO_3 as a supporting electrolyte. We estimate that the pH of these solutions was between 6–7, but was not controlled with a buffer. Table S1 presents the flat band potential (E_{fb}), conduction band (E_{cb}) and valence band (E_{vb}) energies, and the charge carrier density (N_d). Equation S1 relates the capacitance of the space charge region (C_{SC}) to the potential of an electrode versus a reference (E):[6]

$$\frac{1}{C_{SC}^2} = \frac{2}{q\,\varepsilon\,\varepsilon_0\,N_d\,A^2}(E - E_{fb} - \frac{k_B T}{q})$$

(S1)

where q is the fundamental charge of an electron, k_B is Boltzmann's constant, ε is the dielectric constant of the semiconductor (11.7 for Si), A is the electrode area (=0.071 cm²), and ε_0 is permittivity of free space. Equation S1 was used to estimate E_{fb} and N_d. The x-intercept of the linear portion corresponds to $E_{fb} + k_B T q^{-1}$. The flat band potentials were –0.64(±0.04), –0.68(±0.02), and –0.68(±0.03) V vs. SCE for $IrCl_6^{2-}$, FcMeOH, and $Ru(NH_3)_6^{3+}$, respectively.

N_d was estimated using the slope of each line. N_d values ranged from 1.2–3.5×10¹⁵ cm⁻³, corresponding to resistivity values of 1.4–3.8 Ω•cm. This is in excellent agreement with the manufacturer's stated resistivity (1–5 Ω•cm).

The conduction band edges were estimated using equation S2:

$$E_{cb} = E_{fb} + k_B T \ln(N_d/N_c)$$

(S2)

where N_c is the is the effective density of states for the conduction band (= 2.8•10¹⁹ for Si),[6] and E_{cb}, E_{fb}, k_B, T, and N_d were previously defined. The range of E_{cb} values was from –0.87 to –0.93 V vs. SCE. E_{vb} was estimated by adding the Si band gap energy (1.1 eV) to the conduction band edge. The range of

valence band edges was from +0.17 to 0.23 V vs. SCE. The relevant figures of merit are summarized in Table S1.
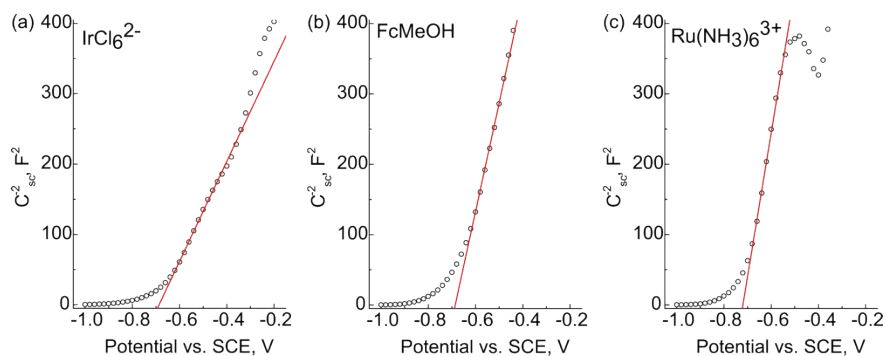
Figure S4. Reciprocal square capacitance versus potential plots for n-Si/Au LAE sensors in (a) $IrCl_6^{2-}$, (b) FcMeOH, and (c) $Ru(NH_3)_6^{3+}$ redox couples. EIS measurements were performed in a three-electrode cell with a SCE reference and glassy carbon rod counter electrode. EIS measurements were made at 50 kHz with an amplitude of 5 mV starting at 0 V and ending at –1 V with a measurement every 20 mV.

Table S1. Summary of Mott-Schottky results acquired using different redox couples. Values represent the mean ± 95% confidence interval for three samples prepared independently.

Redox species[a]	$E_{1/2}$ vs. SCE, V	E_{fb} vs. SCE, V	E_{cb} vs. SCE, V	E_{vb} vs. SCE, V	N_d (×10^{15}), cm^{-3}
$IrCl_6^{2-}$	+0.68	–0.64(±0.04)	–0.87(±0.04)	0.23(±0.04)	3.5(±0.3)
FcMeOH	+0.19	–0.68(±0.02)	–0.93(±0.02)	0.17(±0.02)	1.8(±0.2)
$Ru(NH_3)_6^{3+}$	–0.18	–0.68(±0.03)	–0.93(±0.03)	0.17(±0.03)	1.2(±0.2)
[a] $IrCl_6^{2-}$ = sodium hexachloroiridate (IV); FcMeOH = ferrocene methanol; $Ru(NH_3)_6^{3+}$ = hexaammineruthenium(III) chloride.					

CV measurements were used to confirm fast electron transfer kinetics for FcMeOH and to ensure light addressable behavior. Figure S5 shows CVs of n-Si/Au LAE sensors taken in the dark (black trace) and under illumination (red trace).
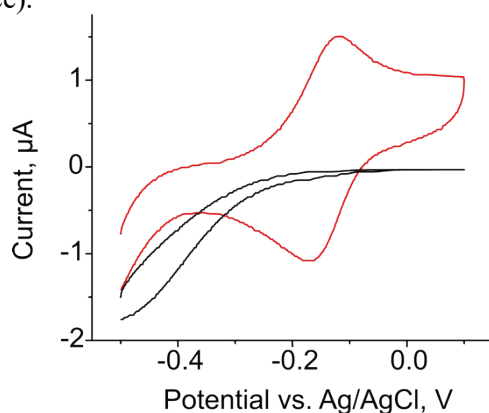
Figure S5. Representative cyclic voltammogram of a 1 mM solution of FcMeOH in 0.1 M KNO_3 using a n-Si/Au LAE sensor. Reference: Ag/AgCl (saturated KCl), Counter: Pt wire, scan rate: 0.1 V s^{-1}, illumination: 85 mW cm^{-2}. Red trace was acquired under illumination, black trace was acquired in the dark.
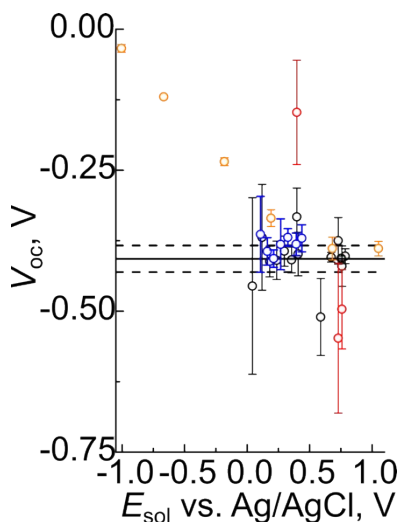
Figure S6. Plot of V_{oc} versus E_{sol} over the range of ±1 V. This figure combines the data in Figures 2f and 3c from the main text and demonstrates that the two methods for determining V_{oc} are consistent.

REFERENCES

1 I. M. Terrero Rodríguez, A. J. Borrill, K. J. Schaffer, J. B. Hernandez and G. D. O'Neil, *Anal. Chem.*, 2020, **92**, 11444–11452.

2 E. G. Arthur, H. Ali, A. Hussain and G. D. O'Neil, *Anal. Chem.*, 2023, **95**, 9219–9226.

3 J. B. Hernandez, Z. B. Epright, I. M. Terrero Rodríguez and G. D. O'Neil, *ChemElectroChem*, , DOI:10.1002/celc.202300400.

4 P. Prod'Homme, F. Maroun, R. Cortès and P. Allongue, *Applied Physics Letters*, 2008, **93**, 21–24.

5 Y. B. Vogel, J. J. Gooding and S. Ciampi, *Chem. Soc. Rev.*, 2019, **48**, 3723–3739.

6 S. Acharya, M. Lancaster and S. Maldonado, *Analytical Chemistry*, 2018, **90**, 12261–12269.